View metadata, citation and similar papers at core.ac.uk
brought to you by CORE
provided by Italian Group Fracture (IGF): E-Journals / Gruppo Italiano Frattura

G. De Pasquale et alii, Frattura ed Integrità Strutturale, 23 (2013) 114-126; DOI: 10.3221/IGF-ESIS.23.12

Scilla 2012 - The Italian research on smart materials and MEMS

Experimental methods for the characterization of fatigue in microstructures

G. De Pasquale, A. Somà
Department of Mechanical and Aerospace Engineering, Politecnico di Torino
Corso Duca degli Abruzzi 24, 10129 Torino (Italy)
aurelio.soma@polito.it, giorgio.depasquale@polito.it

ABSTRACT. The mechanical fatigue behavior of gold microbeams is analyzed. Dedicated devices have been designed and built able to produce alternate loading on gold specimens; the electrostatic actuation is used as driving force. Gold beams are tested under both bending and tensile alternate loadings. Results were used to plot S-N curves and fatigue Goodman-Smith diagram in order to estimate the fatigue limit of the material in presence of mean and alternate stress conditions. The surface topography evolution is studied and failure modes are discussed.

KEYWORDS. Reliability; MEMS; Mechanical fatigue; Gold microbeams; Alternate loading; FEM simulation; Interferometric microscopy.

INTRODUCTION

The reliability of Micro-Electro-Mechanical Systems (MEMS) became a fundamental topic of investigation as a result of their widespread application in many every-day life devices. For instance, micro-fluidic bio-MEMS is used for medical purposes, MEMS-based telecommunication devices are subjected to the action of micro-components as oscillators or switches, inertial sensors for aerospace applications dictate very severe performance requirements in order to minimize repairs and replacement, etc. About structural reliability, it is necessary to examine effects of process parameters, geometry, loads and working environmental conditions, which are all aspects whose knowledge is at present are still under investigation. Electro-mechanical coupling often represents a crucial issue for system reliability even if many other sources of collapse potentially involve reliability. By focusing on material failure, it emerges that mechanical damage represents the more relevant source of failure. Mechanical reliability issues include: mechanical fatigue, thermal fatigue, mechanical strength, surface and contact failure.

A survey of the literature pointed to a lack of experience in investigation of fatigue behavior of metal microstructures; in [1] fatigue testing methods for thin-film metal were described after observing the incidence of material length on damage relative to bulk material. Espinosa [2] evaluated the effect of size on mechanical response of suspended thin gold membranes and described the effect of thickness on yield stress and failure of the membrane investigated fatigue behavior of gold micro-bridges at resonant frequency and pull-in actuation voltage, also monitoring structural stiffness and changes in electrical resistance.

Important parameters for fatigue behavior of gold were investigated and discussed [3] as strain rate sensitivity, grains size, grain boundaries properties and temperature gradients.

FAILURE MODES

Electro-mechanical coupling often represents a crucial issue for the system reliability, especially related to surface contact, corrosion, electromigration and wear. By focusing the attention on the material failure, mechanical damage is the most relevant source of collapse; mechanical reliability issues are concerned with the items listed below:

- ✓ *mechanical fatigue*: devices as micromirrors or microswitches operating at high frequencies and structural components such as hinges or elastic suspensions suffer from cyclic fatigue damage accumulation; cracks initiation and propagation take place in the material and may cause the component failure;
- ✓ *mechanical strength*: the structural integrity of high-stressed components as micro-needles for bioMEMS or thermal posts for microheat exchanges is crucial to avoid fracture collapse;
- ✓ *thermal fatigue*: many sensors and actuators operating by thermal actuation are subjected to relevant temperature gradients and structural strain levels resulting in thermal cycling, high temperature fatigue and creep;
- ✓ *contact surfaces and stiction*: devices including surfaces that come in contact, as microactuators with electrical actuation pads, require a control on the adhesion properties; rotating structures as microrotors situated in microengines need good surface properties resisting wear and stiction.

Failure analysis has an important role in the design, fabrication, and evaluation of performance and reliability of microstructures; some of the most common techniques used for MEMS have been firstly developed for integrated circuits. These techniques include optical and electron microscopy, focused ion beam techniques, atomic force microscopy, acoustic microscopy (to resolve contacts between sticking parts) and scanning laser microscopy.

For moving parts experiencing wear, the most relevant source of failure is represented by sticking of the sliding contacts. The sticking occurs due to changes in the surface topography of the sliding surfaces, which accelerate with an increase in the applied forces. One of the major challenges in failure analysis of MEMS structures has been the inability to duplicate failures [4]. It was reported that failure of some MEMS components are largely due to a single dominant failure mode, e.g., sticking of microengine gears to the substrates or to the hubs [5]. Surface roughening can also cause failure of MEMS structures.

Fatigue failure test results are usually presented in the literature in the traditional form of S-N curves; this requires a high number of failures (represented by a single point of the curve) to draw a single diagram. Another difficulty lies in the fact that the data from S-N curves also capture the device-to-device variability, affected by the uncertainties of material characteristics and fabrication processes. Frequently each investigation involving specific devices tends to be device-dependant; fabrication processes, etching techniques or the substrate material play a major role on film structure strength as well as the presence of initial defects [5, 6].

FATIGUE TESTING STRATEGIES

Mechanical tests for the characterization of fatigue behavior can be divided in two categories according to the experimental configuration used: the "in-situ" configuration adopts on-chip testing machines with specimens that are embedded into the device. The "ex-situ" configuration instead is based on macro-dimensional testing machines [7].

"In-situ" configuration

The first group is the most relevant in the literature and includes simple test structures such as microbeams and microcantilevers, that are largely used for fatigue testing. Some examples are listed in the following: uniaxial cyclic loading tests were performed on single crystal specimens and a reduction in fatigue life was observed for specific strain levels [8]. The fracture caused by fatigue loading on Ni-P amorphous alloy microcantilevers was studied and the fatigue strength resulted about one-third of the static bending strength [9]. From the aspect of fracture striations the authors concluded that the crack propagation occurs by cyclic plastic deformation at the crack tip. Many fatigue experiments were performed on polysilicon resonant structures oscillating in-plane; a perforated plate moved by two sets of comb-drives determines the bending of a notched cantilever [10]. A decay of fracture strength with respect to the single crystal case was documented, together with the correlation between the damage accumulation during crack initiation and the surface oxidation. In the case of gold microbeams specimen design of "in situ" device has been done by the present research group in the last years [11, 12].

"Ex-situ" configuration

Among "ex-situ" experimental configurations, Sharpe [13] described a testing machine for microcantilevers where the actuation force is provided by an external actuator and transferred to the sample through an optical fiber. A mechanical testing device enabling fatigue analyses on microstructures was developed by Komai [14] where single crystal silicon elements were characterized by using an indenter moving in the vertical direction; fracture surfaces were also analyzed by AFM.

TEST STRUCTURES

The "in-situ" excitation strategy was adopted to design and built the test structures used in this work; thus the test structure included the actuator and the sample on a compact geometry. Gold was selected among other ductile materials because of its electrical properties and suitability to simple and low-cost fabrication processes.

Each device for fatigue tests should have the following three features: 1) the possibility to generate variable amplitudes of alternate forces for specimen excitation and variable stress levels inside the material, 2) the possibility to monitor material damage during the accumulation of loading cycles and 3) to provide a criterion to establish the final collapse of the specimen. To identify the exact number of collapses for a given set of specimens, it is fundamental to represent the test results with the established fatigue diagrams as the S−N curve (also known as Wöhler diagram); the number of collapses is also used to estimate the fatigue limit through the "staircase" method. The final collapse is not always identified by the rupture of the specimen but, depending on the specific application, it can be represented by the yielding point, the softening of the material, or other relevant events. In a fatigue test, the event determining the collapse of the specimen must be fixed in advance.

When the test structures for fatigue analysis are designed, a very important parameter that must be determined is the stress level in the specimen. The alternate stress needed to investigate the fatigue behavior is defined by a mean stress σ_m and an alternate stress σ_a. Because of the electro-mechanical strategy was used to load the specimen, the correspondence between actuation voltage and stress level has to be determined in advance, when geometry and shape of the test structure are designed. The appropriate stress levels in the specimen can be obtained by defining appropriately the extension of actuation surfaces, of electrodes gap thickness and structural stiffness. A constant excitation frequency was used to supply the test structures fabricated, so that the excitation signal can be used as a counter of the loading cycles; the number of cycles of excitation was a function of time only.

A test strategy was defined to detect the fatigue behavior of gold samples; the interferometric microscope was used to measure some parameters that were used to estimate the material damage with indirect approach. The strategy described is original and can be extended to general analysis of fatigue in microstructures.

Test structures were built by Bruno Kessler Foundation (Trento, Italy) using the RF switch surface micromachining process and design procedure has been described in previous works [15, 16]. Structural moving parts were obtained through the gold electroplating process; the material was deposited in two steps, allowing the selective superimposition of two gold layers. This permitted creation of thin films of small and large thicknesses, which were used for the specimen and for the suspended actuation electrode, respectively. The thickness of the actuation electrode is higher than that of the specimen to increase its mechanical stiffness; many square holes are present on the suspended electrode to facilitate the chemical removal of the sacrificial layer used to obtain the suspended parts and provide a final 3μm thick air gap. The lower electrode consists of a polysilicon layer deposited on the substrate previously oxidized on the surface and covered with a thin low temperature oxide layer. The material parameters are:

- Young's modulus E = 98.5 GPa
- Poisson ratio ν = 0.42
- Density $\varrho = 19.32 \cdot 10^{-15}$ kg/μm^3

Design 1: shear and flexural fatigue loading

The testing device is shown in Fig. 1a. The nominal geometrical dimensions were checked by the optical profilometer on the actual structures; both nominal and measured dimensions are listed in Tab. 1 for the specimen and the actuation electrode. Figure 1b shows a SEM image of the device. The fatigue test device includes both the actuation electrode that is represented by a perforated plate and the specimen; the specimen is a double-clamped beam with rectangular cross section. The specimen is fixed to a rigid constraint on one side and is connected to the moving plate on the opposite side; plate motion causes bending of the specimen in the out-of-plane direction.

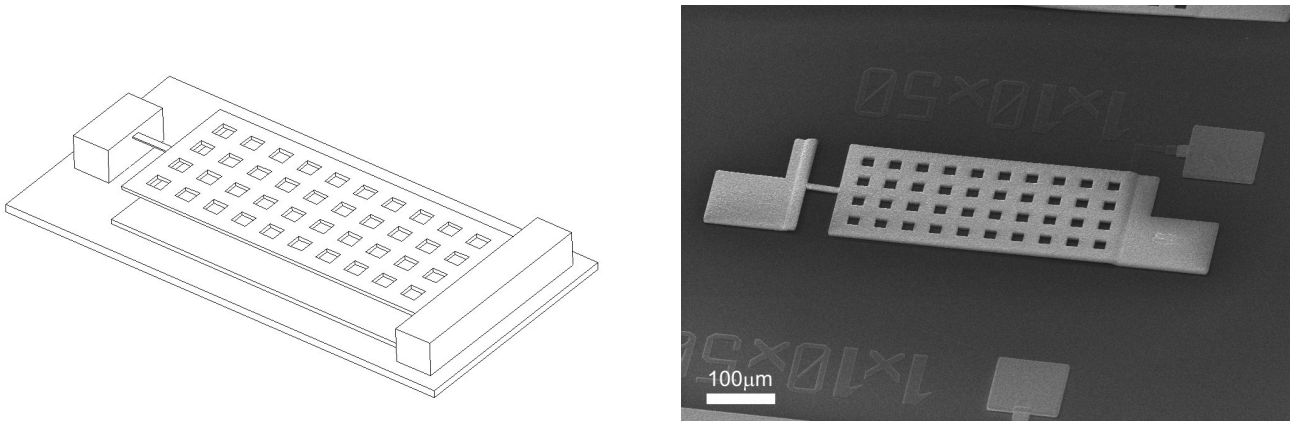

(a) (b)

Figure 1: Geometrical shape of the testing device for shear and flexural fatigue loading with enlarged gap thickness (a) and SEM image of the actual device (b).

At the specimen connections with the rest of the device the sharp corners were rounded to avoid the notch-effect in correspondence with specimen-support and specimen-plate conjunctions. The plate is clamped on the side opposite the specimen. A stress distribution combining shear and flexural components affects the material of the film during its bending; this stress distribution is variable across the beam thickness. The device is supplied by an alternate voltage of actuation that causes the gold beam deflection; the amplitude of the alternate bending force is variable and is proportional to the amplitude of the input voltage. The number of loading cycles can easily be determined by the knowledge of the input voltage frequency and the loading time.

	Nominal dimension [µm]	Measured dimension [µm]
Specimen length	50.0	46.5
Specimen width	10.0	12.4
Specimen thickness	1.800	1.945
Plate length	420.0	417.2
Plate width	180.0	183.1
Plate thickness	4.800	4.695
Holes side	20.0	18.4
Holes interspace	20.0	21.3
Number of holes	10x4	10x4
Lower electrode length	420.0	420.8
Lower electrode width	190.0	192.3
Lower electrode thickness	2.300	2.360
Gap thickness	3.000	3.009

Table 1: Nominal dimensions and dimensions measured by optical profilometer on actual samples for shear and flexural fatigue loading.

Design 2: tensile fatigue loading

The schematic of testing device is represented in Fig. 2a and an optical microscope image of the actual test structure is shown by Fig. 2b. The specimen is the small, suspended double-clamped beam located in the center of the device; the specimen has a rectangular cross section and is connected to the structure with rounded corners to avoid local stress concentration effects. The specimen is connected to two movable plates acting as electrostatic actuators, which are constrained at the outer edges by means of trapezoidal beam elements. The trapezoidal shape is pretty original and was

adopted to provide uniform stress distribution in their material when bend; they act as structural hinges and allows a rigid rotation of the perforated plates. When the plates are actuated, the hinges allow a rigid rotation of the plates around an axis corresponding to the outer constraints, and the specimen undergoes a tensile load. The combined symmetrical rotation of the plates causes a tensile actuation of the specimen situated at the center of the device. Nominal dimensions and effective dimensions of test structures are reported in Tab. 2; the measures were taken with the optical profilometer. The differences between measures are due to the building process tolerances.

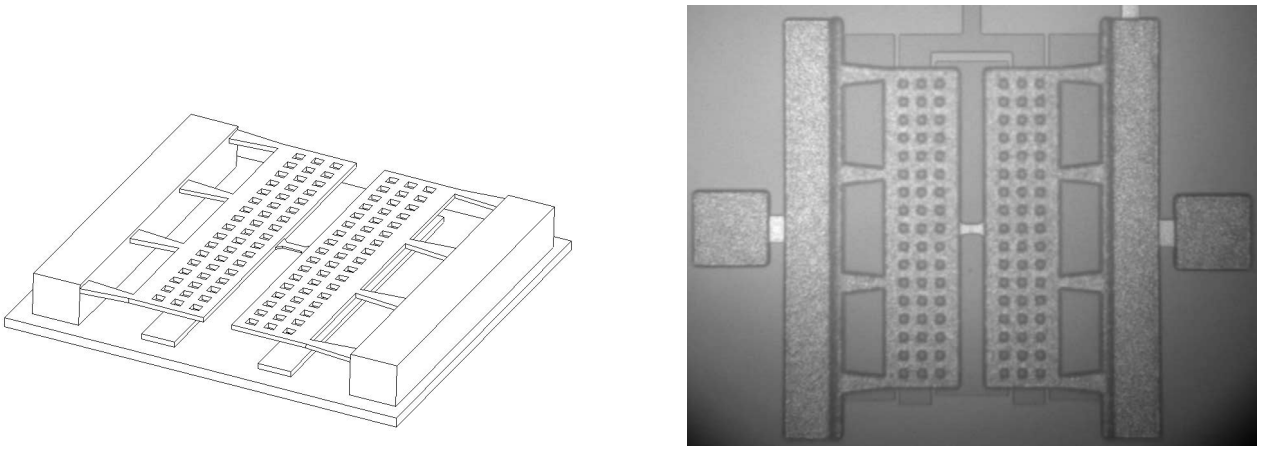

(a) (b)

Figure 2: Geometrical shape of the testing device for tensile fatigue loading where the gap thickness is enlarged (a) and SEM image of the actual device (b).

	Nominal dimension [µm]	Measured dimension [µm]
Specimen length	30.0	27.7
Specimen width	10.0	11.2
Connection radius	4.0	4.0
Plate length	450.8	457.8
Plate width	85.0	84.3
Holes side	8.0	7.8
Number of holes per plate	22x3	22x3
Supports length	50.0	48.2
Supports internal width	15.0	12.8
Supports external width	25.0	23.2
Lower electrode width	105.0	105.0
Internal electrodes distance	85.0	84.7
Specimen thickness	1.800	1.900
Plate thickness	5.400	5.450
Supports thickness	5.400	5.450
Lower electrode thickness	2.300	2.360
Air gap thickness	4.500	4.500

Table 2: Nominal dimensions and dimensions measured by optical profilometer on actual test structures for tensile fatigue loading.

FEM MODELS

The specimen design activity was supported by numerical simulations implemented using a commercial-type tool (ANSYS) for optimizing test device geometry. The nonlinear relationship between structural and electrical domains, due to electrostatic force depending on the local gap width, was modeled by 1-D multiphysics elements

"trans126". A different simulation approach was also used to calculate the stress distribution in the specimen; in these models the structural domain was only represented and the vertical deflection was imposed as a constraint according to the values of deflection measured on actual devices. This approach avoids the uncertainties introduced by the electro-mechanical coupling and gives a precise indication about the stress configuration in the material for a given deformed configuration of the test structure. The estimation of stress distribution refers to an ideal geometry with surfaces unaffected by microdefects; stress distribution in actual specimens depends on crack nucleation points where local stress intensity is amplified, resulting in fatigue-induced failure. Figure 3a shows the results of FEM simulations on the design 1, where the electro-mechanical coupling was included in the model. The same results for the design 2 are represented in Fig. 3b.

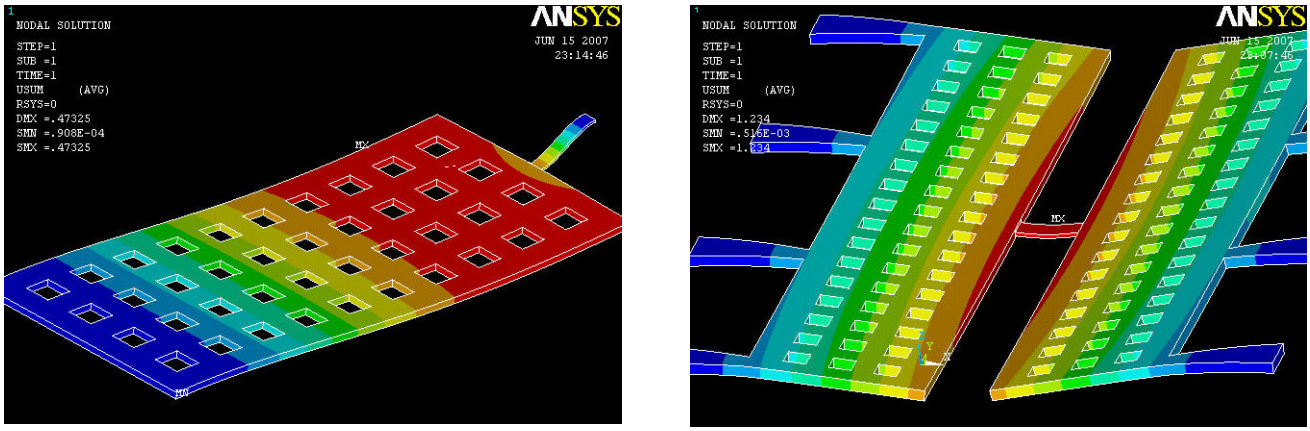

(a) (b)

Figure 3: FEM Von Mises equivalent stress distribution on the devices for shear and flexural (a) and tensile (b) fatigue loading.

Furthermore, dynamic models were used to determine the numerical resonance frequency of the device and to investigate the modal shape of the structure; at this purpose modal analyses of the unloaded structures were performed.

EXPERIMENTAL STRATEGY

Voltage-stress characteristics

The structural analysis was performed under the hypothesis of linear elastic behavior of the material; this assumption is justified by the field of operations that is quite lower than the yield stress level, by the properties of metals, and by the small deformations involved. Despite the specimen shape is very simple, the traditional beam theory supported by an analytic approach is not easy to use in this case. The actuation force is applied to the specimen through movable structures that are subjected to the electro-mechanical coupling lows. As a consequence, a combination of FE simulations and static measurement of the displacement are needed to calculate the stress level in the material with an appreciable confidence. Other effects, such as geometrical features like connection radii, make the numerical approach particularly effective for the analysis.

The static relationship between the applied voltage and specimen tip displacement was measured on actual samples for the design 1 and is shown in Fig. 4. The internal stress of the material was estimated using structural FE models, where the specimen tip displacement was imposed on the basis of the measured values. In order to impose the desired stress levels to the structure during fatigue tests, the characteristics of conversion between electric voltage and stress is needed. This conversion curve was determined in two steps: firstly the relation between electric voltage and static deflection was measured, and then the correspondence between the deflection and the stress distribution was calculated by the FE modeling.

The static voltage-displacement relation was modeled by FEM also, by introducing the experimental values of displacement as constraints; the characteristic that results from the numerical model, compared to the measurements is represented in Fig. 5 for the tensile loading device (design 2).

Then the stress distribution in the specimen was calculated using the previously reported nominal material parameters. Figure 6 represents the relation between the applied static voltage and the maximum stress level in the axial direction of

the specimen; as expected the curve follows a second-order polynomial equation, which is directly dependent on the capacitive voltage-displacement relation. The relation between displacement and stress is linear as a consequence of the linear elastic material characteristic assumed in the FEM model; this assumption is well justified considering the small displacements involved.

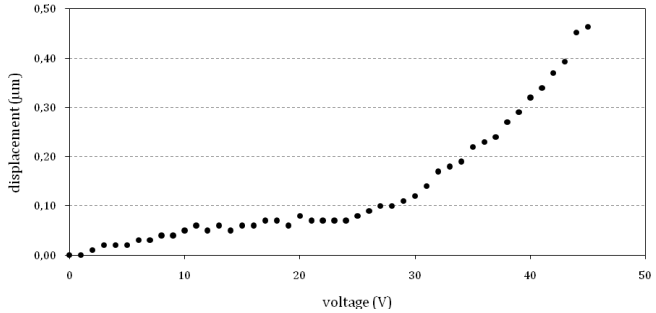

Figure 4: Vertical displacement of the specimen loaded tip measured using the optical interferometric technique with respect to static input voltage (design 1). Measures are affected by an error introduced by surface roughness, particularly at small displacements.

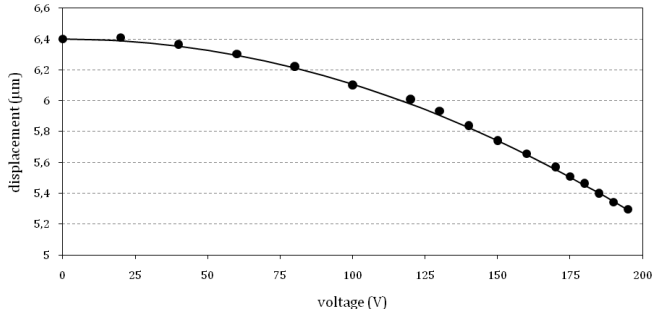

Figure 5: Static voltage-displacement conversion curve for the tensile loading device from FEM simulations (continuous line) and measurements (black dots).

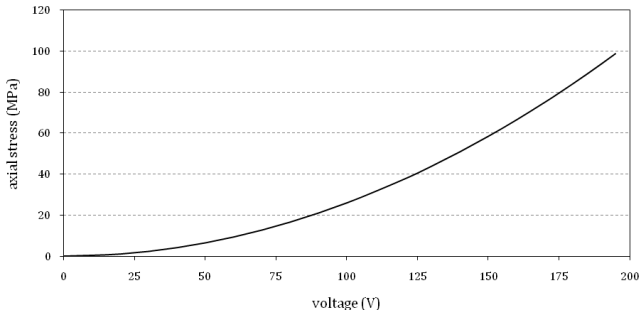

Figure 6: Static voltage-stress conversion curve for tensile loading device (design 2) from FEM simulations constrained with experimental values of deflection.

Experimental setup

A voltage generator was used to supply the test structures; the alternate load causing fatigue was provided by the application of an alternate voltage to the actuators. The number of loading cycles was calculated from the frequency of the actuation voltage. The experiments were performed with the optical interferometric microscope ZoomSurf3D fabricated by Fogale Nanotech (Nimes, France); the same equipment was used for the preliminary static and dynamic measurements previously described [18]. The microscope is equipped by a voltage generator for dynamic tests. The excitation voltage generated may vary in the range 0-200V at low and high frequencies up to 2MHz.

The pull-in voltage as damage detector

Fatigue tests of MEMS reported in the literature show that several different parameters for monitoring material damage can be used. Resonant frequency, quality factor, and electrical resistance are widely used parameters for this purpose. This

work proposes a new strategy for detecting structural stiffness loss, based on the pull-in voltage of the fatigue test device. Because of its sensitivity and ease of setting up the associated experimental equipment, this can be a very significant parameter.

The diagram shown in Fig. 7 represents the equilibrium points between the electric and elastic forces acting on the device. The electric force attracts the actuators towards the corresponding counter electrode, and the elastic force is generated by the structural reaction after deformation and tends to restore the original configuration. The pull-in voltage is the highest level of the actuation voltage that preserves the equilibrium condition under the two forces. The x-axis of the diagram indicates the vertical displacement normalized to the initial gap h_0, while the y-axis represents the electrostatic actuation force (F_{el}) and the elastic reaction of the structure (F_{st}). The elastic curve is variable during the fatigue test because the structural stiffness is affected by the progressive material damaging; thus the slope of the elastic characteristic decreases progressively as the fatigue cycles increase. This means that the value of pull-in voltage varies during the test because the structural stiffness also varies depending to the material damage produced by fatigue. According to the experimental procedure proposed, the change in mechanical stiffness serves as a damage detector in the material and is measured indirectly by monitoring the pull-in voltage.

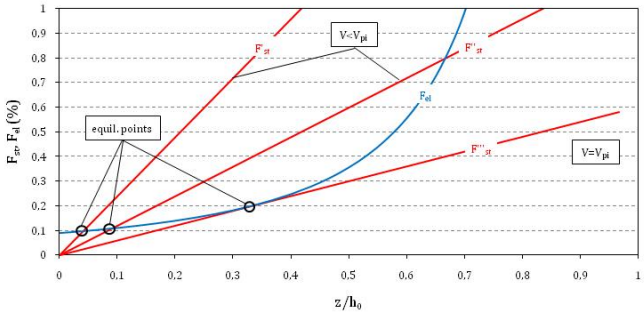

Figure 7: Relation between structural elastic force and electrostatic force; the stiffness variation causes different values of pull-in voltage.

Testing procedure

The test structures are excited by imposing an alternate voltage difference between the lower electrodes and plates; this produces the repetitive movement of the structure and the specimen axial loading. The loading voltage used is identified by three parameters: a) the voltage amplitude V_a, b) the voltage bias V_{bias}, and c) the excitation frequency f. The fatigue test procedure consists of the application of a cyclical loading voltage characterized by a specific set of parameters. The combination of parameters (a) and (b) determines the entity of two additional parameters identifying the stress variation inside the specimen material: the alternate stress σ_a and the mean stress σ_m.

The combination of time and frequency yielded the number of cycles of the current excitation block. The procedure was repeated up to a specimen failure. The failure event was defined in advance as a drastic reduction (at least 10% of the previous value) of the pull-in voltage, reflecting a reduction of the structural stiffness. The pull-in voltage (step 1) was measured by a static actuation using a DC voltage, which was progressively increased. The pull-in condition was detected optically using the interferometer microscope. The alternate load was obtained (step 2) by means of the alternate voltage V_a at 20kHz; the frequency of actuation was set to a value that was significantly lower than the mechanical resonance of the device, which is 28kHz approximately. The two main reasons for this are given as follows:

- the resonant amplification involves additional problems when evaluating material internal stresses;
- the progressive damage in the material could cause a shift in resonance peak or alter the device quality factor as a consequence of possible changes in structural stiffness and damping.

Computing of cycles number

System dynamics must carefully be considered when supply voltage frequency is converted to a number of cycles of alternate load. The force that is responsible for specimen oscillation is generated by the potential difference between suspended and lower electrodes.

For the solution adopted in design 1, two periods T_L of the loading curve correspond to one period T_V of the alternating voltage curve, as represented in Fig. 8. This is due to the electrostatic force that acts always in the attractive direction for both possible polarizations of the electrodes; a consequence is that the current mode of deflection does not allow

oscillation around the undeformed shape. The resulting number of load cycles N_L is related to the number of cycles of alternating voltage N_V according to

$$N_L = 2N_V \tag{1}$$

From this consideration, the number of loading cycles for each step of actuation is

$$n_i = 2ft_i \tag{2}$$

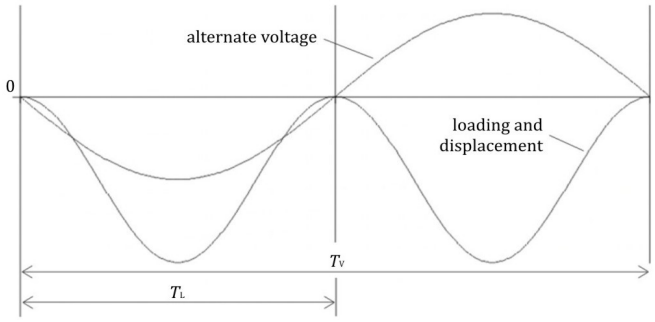

Figure 8: Comparison between actuation voltage cycle and fatigue load cycle for design 1.

The total number of fatigue cycles up to failure can be calculated as

$$N_f = n_1 + ... + n_i + ... + n_m \tag{3}$$

where n_m indicates the number of loading cycles in the last step before collapse. The curves of alternate displacement and local stress have the same frequency as the loading curve. The alternate excitation was maintained for 10 s during the tests between two consecutive measurements of the pull-in voltage; each block of excitation was composed of $4 \cdot 10^5$ cycles of loading, displacement, and local stress. The number of cycles to failure is indicated as N_f.

For the test structure represented by design 2, the total number of fatigue cycles up to failure can be calculated with the same relation reported in Eq. (3). Again, the force responsible for specimen oscillation is generated by the potential difference between the suspended plates and lower electrodes. However, in this case, it results in one period T_L of the loading curve corresponding to one period T_V of the alternate voltage curve; the structure oscillates around the initial deformed shape determined by the V_{bias} load. The resulting number of loading cycles N_L corresponds to the number of cycles of the alternate voltage N_V:

$$N_L = N_V \tag{4}$$

From this consideration, the number of loading cycles for each step of actuation becomes

$$n_i = ft_i \tag{5}$$

RESULTS

Fatigue limit

For the shear micro specimen the fatigue limit was estimated using the "staircase" method; this procedure is largely used in the macroscale to estimate the fatigue limit through a limited number of tests and is widely described in [17]. The "staircase" method is based on a few parameters: the reference number of cycles N_{ref}, the starting load level F, and the load step ΔF. The procedure can briefly be described in a few steps: the first specimen is loaded at the starting load level (F) for N_{ref} cycles; if the specimen collapses during fatigue loading, then the second specimen will be loaded at F–ΔF level for N_{ref} cycles. Instead, if the first specimen does not collapse during fatigue loading, then the second specimen will be loaded at F+ΔF level for N_{ref} cycles. The procedure must be repeated for many specimens by increasing the load level after each nonfailure and by reducing the load level after each failure.

For example, for shear and flexural samples (test structure design 1), the reference number of cycles used was $N_{ref} = 2 \cdot 10^6$, the starting load level was F = 15V, and the load step was ΔF = 1V. The procedure was repeated for six specimens; in Tab. 3, each failure was then reported as 1, while each nonfailure was reported as 0. The fatigue limit

estimated by the application of the "staircase" method is found to be F_D = 13±0.7V. This value was used as an important reference when the alternate-load level was imposed in fatigue tests. According to the definition of fatigue limit, failures at load levels higher than F_D and nonfailures at load levels lower than F_D are normally expected.

Loading level	Specimen 1	2	3	4	5	6
15V	1					
16V		1		1		
17V			0		1	
18V						0

Table 3: Results of fatigue loading on six specimens (design 1) for the fatigue limit estimation using the "staircase" method. The specimen failure is indicated as 1, while the specimen nonfailure is indicated as 0.

Shear and flexural fatigue tests

The results on test structure design 1 are reported in Fig. 9, where the evolution of pull-in voltage for different specimens during the accumulation of load cycles is shown. Each curve refers to a different value of the alternate input voltage used (V_a). The failure was assumed to occur in the instant when the pull-in voltage shows a reduction that is equal to or higher than 10% of the previous value; only collapsed specimens are represented by the curves reported. The curves shown in Fig. 10 indicate the pull-in voltage variation measured on other specimens; some of them failed instantly because of high loading amplitudes (21 and 22.5V); other specimens did not fail after 200 million cycles because they were excited at a load level that is equal or lower than the fatigue limit (10–13V).

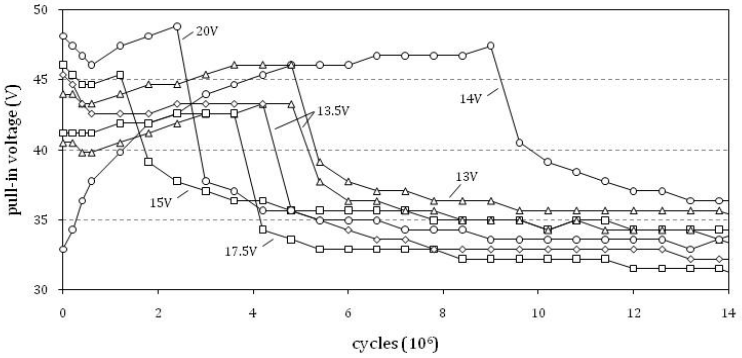

Figure 9: Pull-in voltage of different testing devices (design 1) during the accumulation of fatigue loading, with alternate load being provided at 20kHz frequency at the amplitude V_a indicated for each curve. The pull-in voltage was measured and stored at specific time intervals. The specimen failure is indicated by the strong pull-in reduction (ranging from 12.9% and 22.7% of its last value).

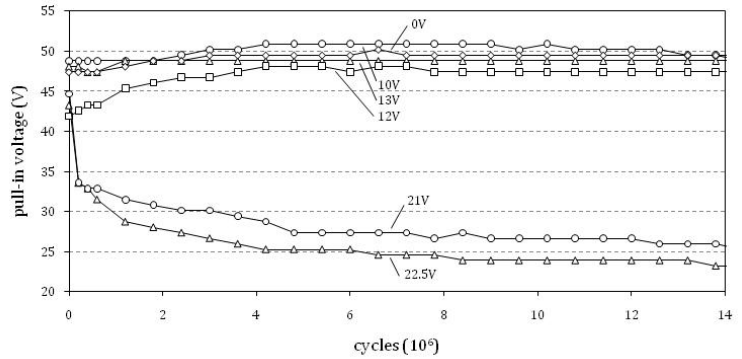

Figure 10: Pull-in voltage of different testing devices (design 1) during the accumulation of fatigue loading, with alternate load being provided at 20kHz frequency at the amplitude V_a indicated for each curve. The pull-in voltage was measured and stored at specific time intervals. Specimens that failed immediately (V_a = 21V and V_a = 22.5V) or that did not fail (V_a = 10V, V_a = 12V and V_a = 13V) are reported. The curve labeled with V_a = 0V represents the pull-in variation during the application of a series of consecutive static actuations without alternate fatigue loading.

A Wöhler diagram (Fig. 11) was obtained by indicating the instant of failure for specific amplitude of the actuation voltage at the corresponding number of cycles. The S-N curve confirms that the estimated value of the fatigue limit is consistent; in fact, it represents the load amplitude threshold separating collapsed specimens from noncollapsed ones.

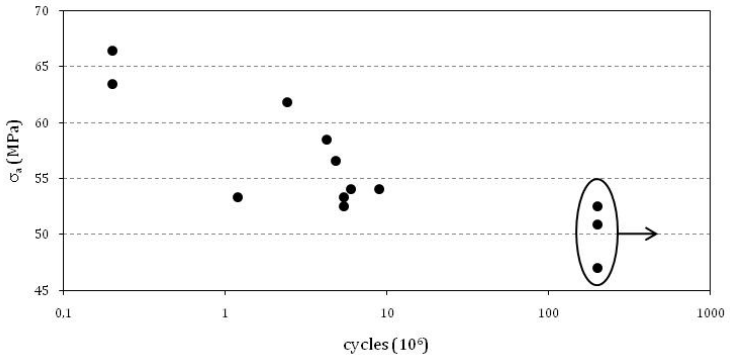

Figure 11: S-N curve (Wöhler diagram) summarizing the results of fatigue tests on shear and flexural specimens. The number of cycles to failure is reported for each specimen in relation to the axial stress amplitude calculated by the FEM model.

Tensile fatigue tests

The stress level produced in the specimen material (test structure design 2) by the electric supply during the fatigue tests was carefully considered; previously extracted and reported voltage-displacement relations were used to properly set the power supply in order to reach the desired levels of mean and alternate stress. Specifically, three different levels of tensile mean stress were produced at 50, 60, and 65MPa, respectively. Table 4 summarizes the loading and stress conditions for each test; the stress level acting along the axial direction of the specimen is reported here as estimated by FEM simulations.

Specimen	σ_m [MPa]	σ_a [MPa]	σ_{max} [MPa]	σ_{min} [MPa]	V_m [V]	V_a [V]	N_f [10^6]
I.1	50	50.0	100.0	0	98.2	98.2	37.2
I.2		46.7	96.8	3.4	114.5	78.5	19.2
I.3		43.8	93.8	6.2	119.5	70.5	28.2
I.4		40.7	90.8	9.4	123.5	63.5	> 45
I.5		36.0	86.0	14.0	127.8	54.3	> 45
II.1	60	41.4	101.4	18.7	141.3	56.4	1.8
II.2		37.7	97.8	22.3	143.3	50.7	8.4
II.3		32.7	92.8	27.3	145.8	43.3	6.6
II.4		28.9	88.9	31.1	147.3	37.8	28.2
II.5		23.9	83.9	36.2	148.9	30.9	> 45
II.6		19.5	79.6	40.5	149.9	25.1	> 45
III.1	65	10.0	75.1	55.0	157.7	12.2	-
III.2		4.0	69.0	61.0	158.1	4.8	19.2
III.3		2.4	67.5	62.6	158.2	2.9	28.2
III.4		1.5	66.5	63.5	158.2	1.8	> 45
III.5		0.8	65.8	64.2	158.2	1.0	> 45

Table 4: Stress levels and actuation voltages used for tensile tests.

Fatigue test results are shown in the S-N diagram of Fig. 12. Each point indicates the number of cycles at which the specimen collapses and the respective amplitude stress level; three levels of mean stress are indicated. The non-failed specimens are marked with a circle. In Fig. 13 the same fatigue results are reported in a Goodman-Smith diagram where the minimum, mean, and maximum stresses are indicated. White dots represent failed specimens, and black dots represent non-failed specimens. The stress levels situated between failure and non-failure stress levels represent the threshold of σ_a (for a given σ_m), under which the component is not sensitive to fatigue phenomenon. The number of cycles $N_{ref} = 45 \cdot 10^6$

was assumed as a reference for identifying non-collapsed specimens: all specimens reaching the N_{ref} number of cycles were assumed to be not sensitive to fatigue under the applied loading conditions. The static voltage used among the successive alternate excitations to test for the integrity of the structure was V_{st} = 100V. The diagram shows trend lines derived from the experimental results; according to the Goodman-Smith theory [16], it is possible to predict roughly the values of ultimate stress (around 110MPa), yield stress (around 75MPa), and fatigue limit at $\sigma_m = 0$ (around 60MPa).

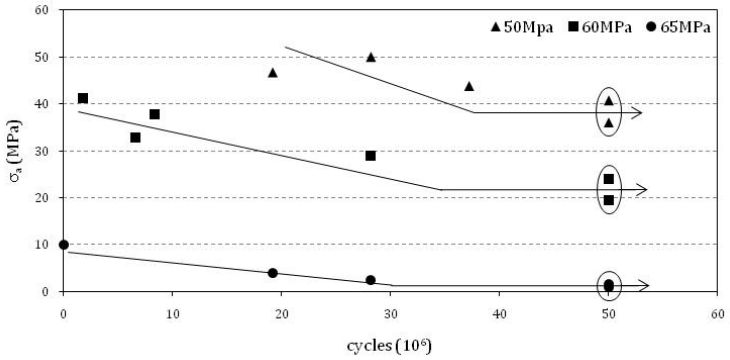

Figure 12: Experimental results of tensile fatigue tests in S-N diagram for three values of mean stress; specimens marked with an arrow do not fail.

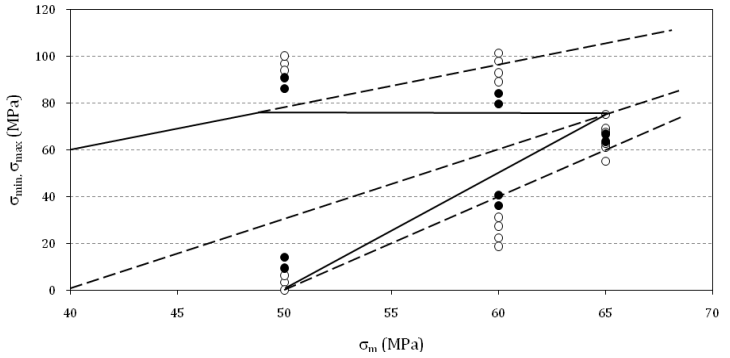

Figure 13: Goodman-Smith diagram of tensile fatigue test results. Failed specimens are indicated with white dots and non-failed specimens with black dots; trend lines are also shown.

DISCUSSIONS

In structures for shear and flexural fatigue tests, the static voltage input used to measure the pull-in of the device did not produce plastic deformations or local yield; this was verified by imposing a series of successive static actuations on the specimen and storing the corresponding pull-in voltage. The resulting curve is shown in Fig. 10 and marked with a 0V amplitude. The value of pull-in results is constant despite several static actuations, revealing that the mechanical characteristics of the device did not change significantly; this leads to the evidence that the material is loaded within the elastic field and, more specifically, that the structural stiffness of the specimen is not affected by the static actuation. Being the experimental strategy based on the correspondence between structural stiffness and material damage, it is evident that the sensitivity of the strategy used is related to the ability to detect the stiffness variation by means of the pull-in voltage.
Similarly, also in structures for tensile fatigue tests (design 2) the static voltage V_{st} used to monitor the material strength was chosen after verifying the safety of the structure under such loading: Fig. 14 shows two voltage-displacement curves measured on the same structure under two consecutive static actuations. The correspondence between the two curves leads to the conclusion that the applied voltage V_{st} = 100V, later used to detect the material strength, is not responsible for stiffness variation and so does not contribute to the material damaging process.
The effect of mean stress on the fatigue behavior was studied by tensile tests, where the application of a bias voltage to the structure allowed introducing a non-symmetric alternate load. When the mean stress of the fatigue load is null, the portions of the loading curve producing a tensile stress and a compression stress in the sample are equal. Instead, in presence of a positive mean stress, the tensile stress condition prevails and determines an increased material degradation.

As the curves reported in Fig. 12 testify, higher is the mean stress level, lower is the number of cycles to failure in presence of a given stress amplitude. The presence of a non-zero mean stress is common in real applications of vibrating microstructures, where electric or mechanical static loads may easily occur.

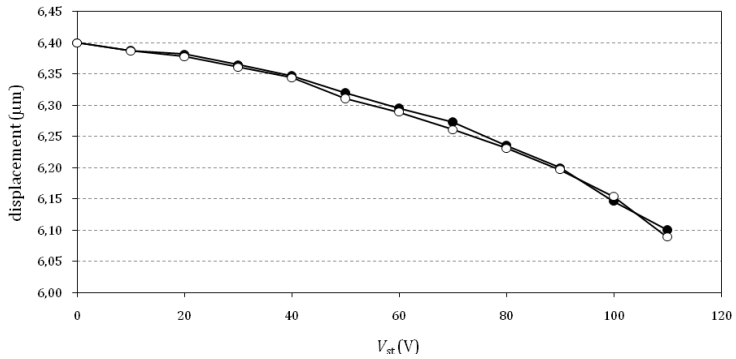

Figure 14: Static displacement of the structure (design 2) under two consecutive actuations; the material was excited in its elastic field.

CONCLUSIONS

The mechanical fatigue of gold MEMS structures was investigated but in the case of alternate stress and in the case of alternate stress with the presence of mean stress. The design of dedicated test structures, supported by FEM simulations addressed to the investigation of stress distribution was introduced. An original experimental strategy was adopted, which relates the stiffness loss and the pull-in voltage to the material damaging. Experimental fatigue results were provided for shear, flexural and tensile loadings. Results has been reported in the classical fatigue graph of Wholer curves and Goodman- Smith graphs. Results on specimen allow to determine important material fatigue parameters for MEMS design procedures.

REFERENCES

[1] G.P. Zhang, R. Schwaiger, C.A. Volkert, O. Kraft, Philosophical Magazine Letters, 83 (2003) 477.
[2] H.D. Espinosa, B.C. Prorok, B. Peng, ", J. of the Mechanics and Physics of Solids, 52 (2004) 667.
[3] Y.H. Chew, C.C. Wong, F. Wulff, F.C. Lim, H.M. Goh, Thin Solid Films, 516 (2008) 5376.
[4] D.M. Tanner, In: Proc. 22nd Int. Conference on Microelectronics, Piscataway, USA, (1999) 97.
[5] A.B. Soboyejo, K.D. Bhalerao, W.O. Soboyejo, J. of Materials Science, 38 (2003) 4163.
[6] H.D. Espinosa, B.C. Prorok, J. of Materials Science, 38 (2003) 4125.
[7] S.M. Allameh, J. of Materials Science, 38 (2003) 4115.
[8] T. Ando, S. Mitsuhiro, K. Sato, Sensors and Actuators A: Physical, 93 (2001) 70.
[9] S. Maekawa, K. Takashima, M. Shimojo, Y. Higo, S. Sugiura, B. Pfister, M.V. Swain, Japanese Journal of Applied Physics, 38(1999) 7194.
[10] C.L. Muhlstein, S.B. Brown, R.O. Ritchie, Sensors and Actuators A: Physical, 94 (2001) 177.
[11] A. Somà, G. De Pasquale, J. of Microelectromechanical Systems, 18(4) (2009) 828.
[12] G. De Pasquale, A. Somà, A. Ballestra, Analog Integrated Circuits and Signal Processing, 61 (2009) 215.
[13] W.N. Sharpe, J. Bagdahn, Mechanics of Materials, 36 (2004) 3.
[14] K. Komai, K. Minoshima, S. Inoue, Microsystem Technologies, 5 (1998) 30.
[15] A. Somà, G. De Pasquale, In: International Semiconductor Conference (CAS 2007).
[16] G. De Pasquale, A. Somà, J. of Microelectromechanical Systems, 20(4) (2011) 1054.
[17] J. A. Collins, Failure of materials in mechanical design. Analysis, Prediction, Prevention, New York, Wiley Interscience, (1993).
[18] G. De Pasquale, A. Somà, Microsystems Technologies, 15 (2009) 391.